Available online at www.sciencedirect.com
ScienceDirect
Journal of Luminescence 124 (2007) 39–44
JOURNAL OF LUMINESCENCE
www.elsevier.com/locate/jlumin

Preparation and luminescent properties of europium-doped yttria fibers by electrospinning

Hongquan Yu[a,b], Hongwei Song[a,*], Guohui Pan[a,b], Suwen Li[a,b], Zhongxin Liu[a,b], Xue Bai[a,b], Tie Wang[a], Shaozhe Lu[a], Haifeng Zhao[a]

[a]*Key Laboratory of Excited State Physics, Changchun Institute of Optics, Fine Mechanics and Physics, Chinese Academy of Sciences, 16 Eastern Nan-Hu Road, Changchun 130033, PR China*
[b]*Graduate school of Chinese academy of Sciences, PR China*

Received 20 September 2005; received in revised form 18 January 2006; accepted 26 January 2006
Available online 22 March 2006

Abstract

Sub-micrometer-sized fibers of europium-doped yttria (Y_2O_3:Eu^{3+}) were prepared by electrospinning followed by high-temperature calcinations for the first time. The fibers were with diameters of 200–400 nm and lengths of several 10 μm and cubic in phase. The spectral properties of the Y_2O_3:Eu^{3+} fibers were studied, in contrast with those of bulk powders. The results indicated that in the present Y_2O_3:Eu^{3+} fibers the excited charge transfer band had slightly blue shift in comparison with that in the bulk due to weaker covalence of Eu–O bonds. In addition, both of the lifetimes of the $^5D_1$ and $^5D_0$ states in the fibers became shorter than that in the bulk due to improved nonradiative transition rates.

PACS: 78.55.−m; 78.67.−n

Keywords: Y_2O_3:Eu^{3+}; Electrospinning; Fibers; Luminescent properties

1. Introduction

In recent years, much attention has been paid to the preparation and characterization of one-dimensional (1D) nanomaterials because of their unique physical and chemical properties [1–3]. Many unique and fascinating properties have been proposed and demonstrated for this class of materials, such as metal insulator transition [4], superior mechanic toughness [5], higher luminescent efficiency [6,7], enhancement of thermoelectric figure of merit [8] and lowered threshold [9].

Rare-earth-doped materials are an important type of phosphors due to their excellent performance, which have been intensively applied in many areas, such as high-performance magnets, luminescence devices and catalysts. Most of these functions depend strongly on the composition and structure of materials. In recent years, researches on nanosized phosphors doped with rare-earth ions have attracted a great deal of attention [10–12]. Meyssamy et al. [13] synthesized rate-earth ion (Tb^{3+}, Ce^{3+}) doped $LaPO_4$ nanowires for the first time and reported their luminescent properties . Compared with zero-dimensional nanoparticles, the shape of anisotropy of a 1D structure provided a better model system to investigate the dependence of electronic transport and optical properties on size confinement and dimensionality. In one of our previous works, we observed that the luminescent quantum efficiency of $^5D_1$–$\sum^7F_J$ transitions of Eu^{3+} in $LaPO_4$ nanowires was enhanced more considerably than that of the corresponding nanoparticles and the bulk powders [14]. Y_2O_3:Eu^{3+} is an important doped compound for many phosphor applications such as in plasma display panels and in fluorescent lamps [15]. Many methods have been mentioned in literature to prepare Y_2O_3:Eu^{3+} 1D nanostructures such as using anodic aluminum oxide template [16],

*Corresponding author. Tel./fax: +86 431 6176320.
E-mail address: hwsong2005@yahoo.com.cn (H. Song).

0022-2313/$ - see front matter © 2006 Elsevier B.V. All rights reserved.
doi:10.1016/j.jlumin.2006.01.360

homogeneous precipitation [17] and hydrothermal treatment [18].

Electrospinning has been extensively explored for fabricating long fibers [19,20]. It has been demonstrated that a variety of materials such as polymers, ceramics, carbons, and composites all can be electrospun to form uniform fibers [20]. Electrospinning involves the application of electrostatic force between a polymer solution kept in a syringe and a metal electrode kept at a suitable distance. With the increase in electric potential the charged pendant drop of polymer solution formed at the tip of the capillary is deformed into a cone, known as "Taylor's cone" [21]. Once the electric field strength has surpassed a threshold to overcome the surface tension, electrostatic force will cause the ejection of a thin, charged jet. The jet ejected from the tip of the capillary undergoes a whipping process, which leads to the formation of ultrathin fibers as a result of solvent evaporation [22]. The fibers can be collected in the form of long threads on the surface of the electrode, the fiber diameters are in the range of a few micrometers to nanometers. In general, the fibers that are deposited on the surface of a conductor form non-woven mats characterized by high surface area and small pore size [22].

At present, there is no literature on the preparation of rare-earth phosphors by electrospinning. It is expected that electrospining will develop as a new technique to prepare nanosized rare-earth phosphors. In this paper, we demonstrate, for the first time to our knowledge, the preparation and luminescent properties of Y_2O_3:Eu^{3+} fibers through the method of electrospinning.

2. Experimental

The schematic diagram of the electrospinning setup is shown in Fig. 1. It consists of three major components: a high-voltage power supply, a spinneret (a needle), and a collector plate (a grounded conductor). For the preparation of the fibers of Europium-doped yttria, 3.0×10^{-3} mol of yttrium acetate and 6.0×10^{-5} mol of europium nitrate in the required molar ratio [$Y(CH_3COO)_3$:$Eu(NO_3)_3$ = 1:0.02 mol ratio] were dissolved in 10.0 g of deionized water. Slowly into the solution 40.0 g of 10 wt% aqueous PVA solution was eye dropped and vigorously stirred in a water bath at 50 °C for 4 h. A viscous solution containing PVA, yttrium acetate and europium nitrate was obtained. The solution was introduced into a plastic syringe 20 cm away from a metal cathode electrode (such as aluminum foil). The positive (anode) terminal of a variable high-voltage transformer capable of delivering 50 kV was attached to a copper wire inserted into the solution in the syringe and the negative terminal was attached to an aluminum foil target electrode. The tip of the syringe was placed at an angle 15° to the horizontal in order to maintain a uniform flow of the solution. A high voltage of 18 kV was applied between the anode and cathode. A non-woven mash of nano-to-micron diameter organic–inorganic hybrid fibers was collected on the surface of the cathode. The as-prepared composite fibers were dried initially 12 h at room temperature under vacuum, then calcined at 200–660 °C with a rise rate of 15 °C/h and kept for 4 h at 660 °C. After calcinations, fibers of pure cubic Y_2O_3:Eu^{3+} were obtained. For comparison, bulk Y_2O_3:Eu^{3+} (1:0.02 in mol ratio) powders were prepared by the solid-state reaction at 1100 °C.

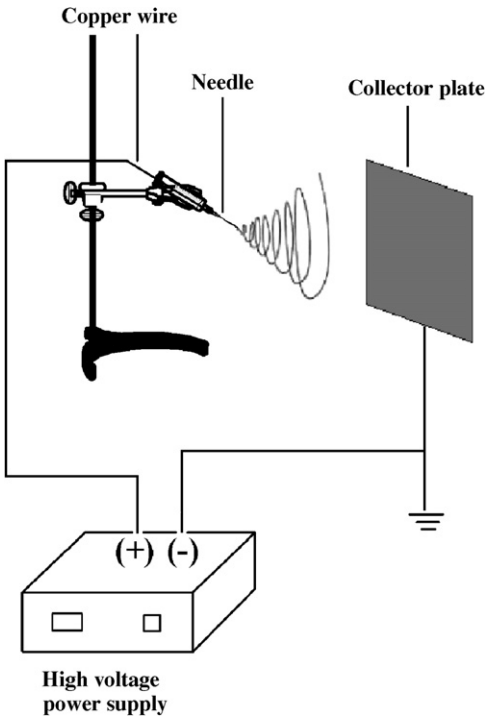

Fig. 1. Schematic diagram of the electrospinning setup.

The morphology of the fibers was inspected using a JOEL JXA-840 scanning electron microscopy and PHILIPS XL30 field emission scanning electron microscope (FE-SEM). X-ray diffraction (XRD) data of the fibers was collected on Rigaku D/max-rA X-ray diffractometer using a Cu target radiation source, scans were made from 25° to 60° (2θ) at the speed of 2° min^{-1}. Fourier transform infrared spectroscopy (FTIR) was recorded in the range of 1100–4000 cm^{-1} on a Fourier transform spectrometer (Perkin-Elmer, Spectrum 1, USA) with a resolution of 1 cm^{-1}. The excitation and emission spectra were recorded at room temperature using a Hitachi F-4500 spectrophotometer equipped with continuous 150 W Xe-arc lamp. In the measurements of time-resolved spectra and fluorescence dynamics, a 266-nm light generated from the fourth harmonic generator pumped by the pulsed Nd:YAG laser was used as excitation source. The YAG:Nd laser has a line width 0.3 cm^{-1}, pulse duration of 10 ns, and repetition frequency of 10 Hz. A Spex 1403 spectrometer, a photon-multiplier and a boxcar intergrator were used for detection of the spectra. Fluorescence dynamics were recorded by a TEKTRONIX TDS-3052 oscilloscope.

3. Results and discussion

The SEM photographs of PVA/yttrium acetate/europium nitrate composite fibers and the fibers calcined at 660 °C are shown in Fig. 2. It can be seen that the as-prepared fibers are of the order of ~500 nm in size and the surfaces of the fibers (Fig. 2a) are smooth. In order to obtain pure ceramic Y_2O_3:Eu^{3+} fibers, the as-prepared materials were subjected to calcinations. During calcination, pure Y_2O_3:Eu^{3+} was formed from yttrium acetate and europium nitrate. The photograph (Fig. 2b) exhibits that the diameters of the fibers obtained after calcination at 660 °C are smaller than those of the composite fibers because of the decomposition of the PVA component. The diameters of the fibers obtained after calcination is in the range of 200–400 nm. The FE-SEM photograph of Y_2O_3:Eu^{3+} fibers is presented in Fig. 2c. The high-resolution images further confirm that the Y_2O_3:Eu^{3+} nanocrystals are 1D. Some pin holes randomly distribute in the fibers.

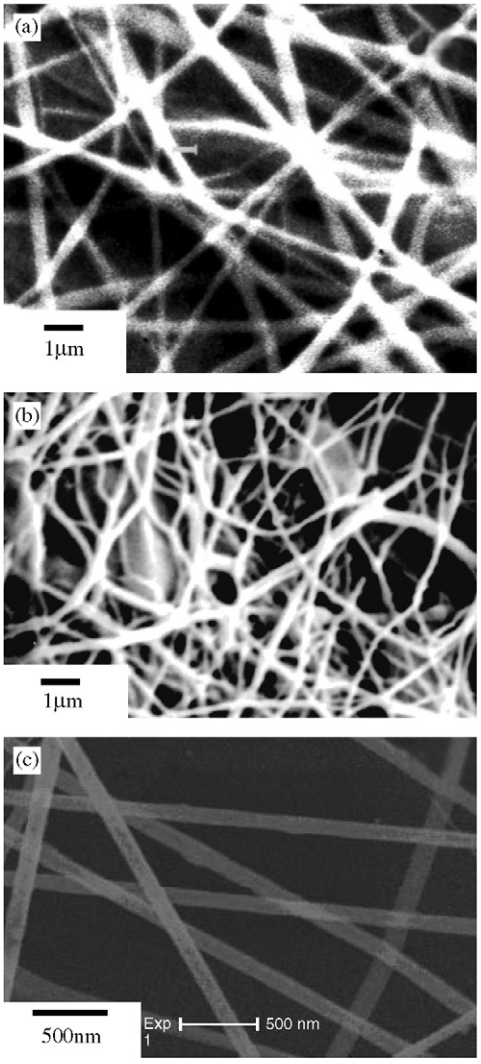

Fig. 2. (a) SEM image of PVA/yttrium acetate/europium nitrate composite fibers, (b) The SEM image of Y_2O_3:Eu^{3+} fibers and (c) FE-SEM image of Y_2O_3:Eu^{3+} fibers.

Fig. 3 shows the XRD patterns of the as-prepared PVA/yttrium acetate/europium nitrate composite and the annealed fibers. The results indicate that the as-prepared fibers are in the amorphous phase. Following the calcination, excellent XRD patterns appeared due to the crystallization of Y_2O_3:Eu^{3+}. The diffraction peaks can be indexed as cubic structure (space group:Ia3) of Y_2O_3 with cell parameters $a = 1.0651$ nm, and the diffraction data are in agreement with the JCPDS card of Y_2O_3 (JCPDS 88-1040). No additional phase was formed. The crystalline size of the nanocrystals composing the fibers can be estimated according to the XRD patterns by using the scherrer relation:

$$D = \frac{k\lambda}{\cos\ \theta\ \Delta(2\theta)},$$

where D is the size of the crystals, k is the Scherrer constant ($k = 0.89$), λ is the wavelength of the X-ray ($\lambda = 0.154$ nm) and Δ is the width at 2θ ($2\theta = 28.99°$). The average crystalline size of Y_2O_3:Eu^{3+} nanoparticle was determined to be ~17 nm, which was much smaller than the size of 1D nanostructures shown in Fig. 2(c). This suggests that the Y_2O_3:Eu^{3+} fibers consisted of multi-nanocrystals or they might be the tight connection of Y_2O_3:Eu^{3+} nanocrystals with diameters of ~17 nm.

Fig. 4a shows the excitation spectra of different Y_2O_3:Eu^{3+} samples at room temperature. The broad band extending from 200 to 300 nm is assigned to the charge transfer (CT) transitions of Eu^{3+}. The CT band of Y_2O_3:Eu^{3+} corresponds to the electronic transition from the 2p orbital of O^{2-} to the 4f orbital of Eu^{3+}, and is related closely to the covalence between O^{2-} and Eu^{3+} and coordination environment around Eu^{3+} [23]. The main peak location of the CT band in the fibers (241 nm) had slightly blue-shift in comparison with that in the bulk powders (244 nm). The increase in energy for electron transfer from O^{2-} to Eu^{3+} represents the decrease in the

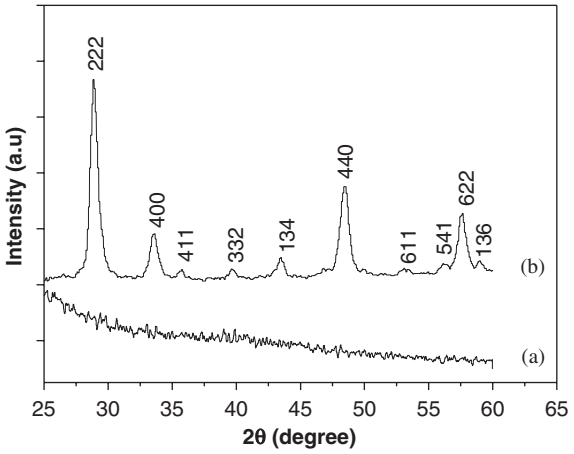

Fig. 3. XRD pattern for the different fibers samples: (a) PVA/$Y(CH_3COO)_3$/$Eu(NO_3)_3$ composite fibers and (b) fibers of Y_2O_3:Eu^{3+}.

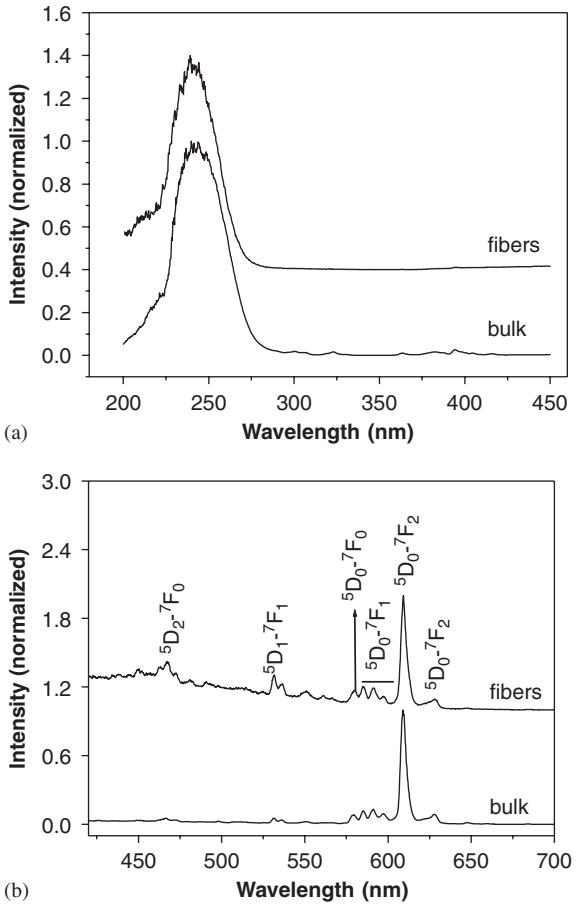

Fig. 4. (a) Room-temperature excitation spectra of Eu^{3+} in different Y_2O_3:Eu^{3+} powders ($\lambda_{em} = 609$ nm), (b) room-temperature emission spectra of Eu^{3+} in different Y_2O_3:Eu^{3+} powders under 241 nm excitation.

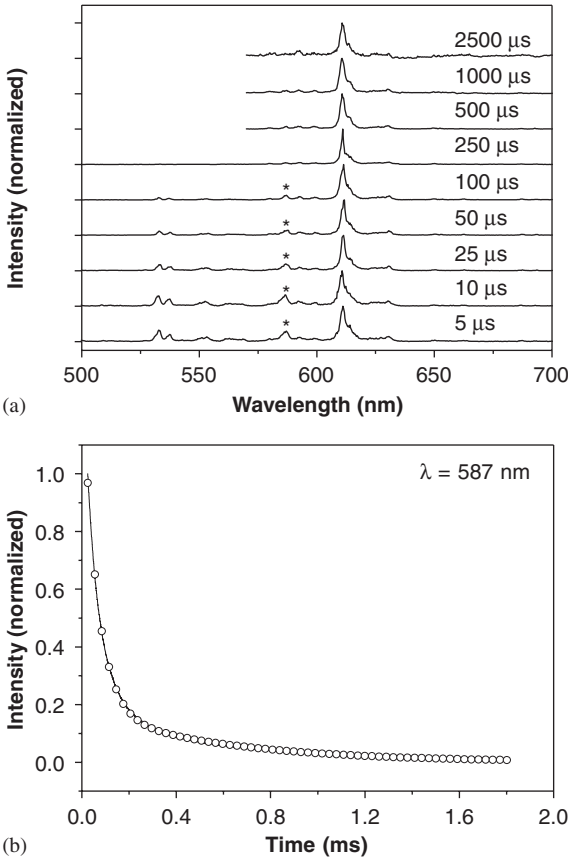

Fig. 5. (a) The time-resolved emission spectra of fibers for different delay times at room temperature. (b) Fluorescent decay curves of $^5D_0$–$^7F_1$ transitions at 587 nm under the 266 nm excitation at room temperature. The solid lines are experimental data, and the circles are fitting functions.

covalence and the increase in ionicity between O^{2-} and Eu^{3+}. It indicates that the covalence of Eu–O bonds in the fibers is a little bit weaker than that in the bulk. Fig. 4b shows the emission spectra of Y_2O_3:Eu^{3+} under the excitation of a 241 nm continuous light. The emission spectrum of fibers not only contains the characteristic transition lines from the lowest excited $^5D_0$ level of Eu^{3+} but also those from higher energy levels ($^5D_1$, $^5D_2$) of Eu^{3+}, as labeled in the Fig. 4. The spectra are described by the $^5D_0$–^7F_J line emissions ($J = 0$, 1, 2, 3, 4) of the Eu^{3+} ion with the strongest emissions for $J = 2$ at 609 nm. The $^5D_0$–$^7F_2$ lines originate from electric-dipole transition and its intensity is sensitive to the local structure surrounding the Eu^{3+} ions, while the $^5D_0$–$^7F_1$ lines originate from magnetic-dipole transition and the change of the crystal field strength has very little influence to the intensity of $^5D_0$–$^7F_1$ transition acting on the Eu^{3+} ion. Therefore, the intensity ratio of the electric-dipole to magnetic-dipole transition is widely used for the study of the chemical bond of anions coordinating the rare earth ions. Smaller the intensity ratio, weaker the covalence of the Eu–O bonds. The intensity ratios of $^5D_0$–$^7F_2$ to $^5D_0$–$^7F_1$ in fibers and bulk were calculated to be 1.98 and 3.12, respectively. This indicates that the covalence of Eu–O bonds in the fibers is weaker than that in the bulk, which is inconsistent with the blue-shift of the CT band.

Fig. 5a shows the time-resolved emission spectra in the Y_2O_3:Eu^{3+} fibers. As labeled in the figure, the lines in the range of 530–570 nm are assigned to the $^5D_1$–$^7F_1$ transitions, and the lines in the range 575–700 nm are assigned to the $^5D_0$–^7F_J ($J = 0-4$) transitions. It can be seen that as the delay time increased from 5 to 100 μs, the intensity of the peak labeled with star (587 nm) decreased dramatically, like the $^5D_1$–$^7F_1$ transitions in the range of 530–570 nm. This indicates that there is a decay time constant in the order of several 10 μs, which is inconsistent with the decay time constant of $^5D_1$. According to the energy levels, we can conclude that the line labeled with star originated from the overlapped $^5D_1$–$^7F_3$ and the $^5D_0$–$^7F_1$ transitions. It should be pointed out that the similar phenomenon was also observed in the bulk Y_2O_3:Eu^{3+} and Y_2O_3:Eu^{3+} nanocrystals prepared by the other techniques. Herein we discuss this point to let one recognize that the contribution of $^5D_1$–$^7F_3$ influences the spectral configuration of $^5D_0$–$^7F_1$. Fig. 5b shows the luminescence decay curve of the line labeled with star. It is obvious that the luminescence decays biexponentially. By fitting, the two time constants

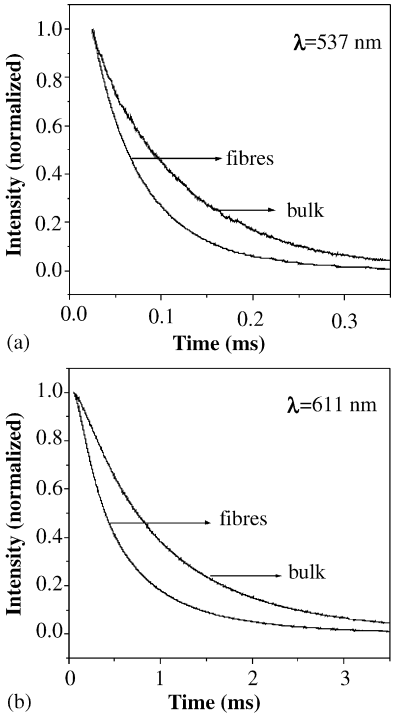

Fig. 6. Fluorescent decay curves of (a) the $^5D_1$–$^7F_1$ transitions at 537 nm and (b) the $^5D_0$–$^7F_2$ transitions at 611 nm of Eu^{3+} in the two samples under the 266 nm excitation at room temperature.

were determined to be 61.4 and 567.2 μs, corresponding to the decay of $^5D_1$–$^7F_3$ and $^5D_0$–$^7F_1$ transition of Eu^{3+}, respectively.

To study the decay behaviors of Eu^{3+} luminescence in more details in the Y_2O_3:Eu^{3+} fibers, the kinetic curves for the representative emission of Eu^{3+} $^5D_1$–$^7F_1$ (537 nm) as well as $^5D_0$–$^7F_2$ (611 nm) in different Y_2O_3:Eu^{3+} samples were measured at room temperature, as shown in Fig. 6. All the curves decay exponentially. The fluorescence lifetimes of $^5D_1$–$^7F_1$ (537 nm) were determined to be 59 μs in fibers and 100 μs in bulk. The fluorescence lifetimes of $^5D_0$–$^7F_2$ (611 nm) were determined to be 560 μs in fibers and 1.01 ms in bulk. It is apparent that in the fibers both the lifetimes of $^5D_1$ and $^5D_0$ became shorter than those in the bulk, suggesting that the total electronic transition rates increase. The lifetime τ can be described as,

$$\tau = \frac{1}{w_R + w_{NR}},$$

where w_R is the radiative transition rate and w_{NR} the non-radiative relaxation rate, respectively. In the present sub-micrometer-sized Y_2O_3:Eu^{3+} fibers, the size confinement does not work at all. In addition, the crystal lattice constant hardly changes. Thus we have reason to consider that the total radiative transition rate of $^5D_0$–$\sum^7F_J$ hardly changes. The decrease of florescence lifetime mainly originates from the increase of nonradiative transition rate. In the present Y_2O_3:Eu^{3+} fibers, more defect states were involved in the preparation, which may act as

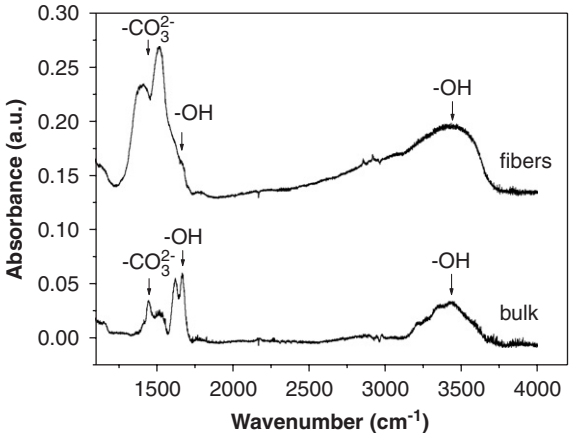

Fig. 7. FTIR absorption spectra of different Y_2O_3:Eu^{3+} samples.

nonradiative relaxation channels. Fig. 7 shows the FTIR absorption spectra of the Y_2O_3:Eu^{3+} fiber in comparison to the bulk. The bands around 3440 and 1650 cm^{-1} are due to the OH stretching and deformation vibrations, respectively. A split band around 1450 cm^{-1} indicates the presence of carbonate group. The existence of these groups should arise from the absorption of H_2O and CO_2. The vibration groups with large energy may act as quench centers, leading to increased non-radiative relaxation rate and shortened lifetime. In Fig. 7 it can be clearly seen that in the Y_2O_3:Eu^{3+} fibers, the vibration of carbonate group increases considerably than that in the bulk. According to the preparation conditions, we suggest that a large number of CO_2 leave in the pin holes of the Y_2O_3:Eu^{3+} fibers with the decomposition of $Y(CH_3COO)_3$. Of course, the surface contamination should be also considered. The Y_2O_3:Eu^{3+} fibers have larger surface-to-volume ratio, which is easier to absorb CO_2 and H_2O in the air.

4. Conclusion

Cubic Y_2O_3:Eu^{3+} nanosized fibers have been successfully prepared using an electrospinning method. The luminescent properties were studied in comparison to the bulk. It was observed that the CT band of Y_2O_3:Eu^{3+} fibers had slightly blue shift in comparison with that in the bulk, indicating that the covalence of Eu–O bonds in the fibers is weaker than that in the bulk. In addition, both of the lifetimes of the $^5D_1$ and $^5D_0$ states in the fibers became shorter than that in the bulk due to improved nonradiative transition rates. Overall, electrospinning is a novel technique to fabricate rare earth photoluminescent fibers.

Acknowledgments

This work is supported by the National Nature Science Foundation of China (Grants 10374086 and 10274083).

References

[1] P.D. Yang, H.Q. Yan, S. Mao, R. Russo, J. Johnson, R. Saykally, N. Morris, J. Pham, R.R. He, H.-J. Choi, Adv. Funct. Mater. 12 (2000) 323.
[2] Y.Y. Wu, H.Q. Yan, M. Huang, B. Messer, J.H. Song, P.D. yang, Chem. Eur. J. 8 (2002) 1260.
[3] J. Hu, T.W. Odom, C.M. Lieber, Accounts Chem. Res. 32 (1999) 435.
[4] J.T. Devreese, R.P. Evrard, V.E. van Doren, Highly Conducting One-Dimentional Solids, Plenum, New Delhi, 1979.
[5] E.V. Wang, P.E. Sheehan, C.M. Lieber, Science 277 (1997) 1971.
[6] L.T. Canham, Appl. Phys. Lett. 57 (1990) 1046.
[7] J.D. Holmes, K.P. Johnston, R.C. Doty, B.A. Korgel, Science 287 (2000) 1471.
[8] L.D. Hicks, M.S. Dresselhaus, Phys. Rev. B 47 (1993) 16631.
[9] Y. Arakawa, H. Sakaki, Appl. Phys. Lett. 40 (1982) 939.
[10] G.A. Hebbink, J.W. Stouwdam, D.N. Reinhoudt, F.C.J.M. Van Veggel, Adv. Mater. 79 (2002) 1147.
[11] H. Song, B. Chen, H. Peng, J. Zhang, Appl. Phys. Lett. 81 (2002) 1776.
[12] L. Yu, H. Song, S. Lu, Mater. Res. Bull. 39 (2004) 2083.
[13] H. Meyssamy, K. Riwotzki, A. Kornowski, S. Naused, M. Haase, Adv. Mater. 11 (1999) 840.
[14] H. Song, L. Yu, S. Lu, T. Wang, Z. Liu, L. Yang, Appl. Phys. Lett. 85 (2004) 470.
[15] C.R. Ronda, J. Lumin. 72–74 (1997) 49.
[16] J. Zhang, G. Hong, J. Solid State Chem. 177 (2004) 1292.
[17] C.F. Wu, W.P. Qin, G.S. Qin, D. Zhao, J.S. Zhang, S.H. Huang, S.Z. Lu, H.Q. Liu, H.Y. Lin, Appl. Phys. Lett. 82 (2003) 520.
[18] Y. He, Y. Tian, Y.F. Zhu, Chem. Lett. 32 (2003) 862.
[19] D. Li, Y. Xia, Adv. Mater. 16 (2004) 1151.
[20] D. Li, G. Ouyang, Y. Xia, Nano. Lett. 5 (2005) 913.
[21] B. Sundaray, V. Subramanian, T.S. Natarajan, R.Z. Xiang, C.C. Chang, W.S. Fann, Appl. Phys. Lett. 84 (2004) 1222.
[22] D. Li, T. Herricks, Y. Xia, Appl. Phys. Lett. 83 (2003) 4586.
[23] X. Bai, H. Song, L. Yu, L. Yang, Z. Liu, G. Pan, S. Lu, X. Ren, Y. Lei, L. Fan, J. Phys. Chem. B 109 (2005) 15236.